# Time-dependent geometry and energy distribution in a spiral vortex layer

J. R. Angilella* and J. C. Vassilicos†
*Department of Applied Mathematics and Theoretical Physics, University of Cambridge, Silver Street, Cambridge CB3 9EW, United Kingdom*
(Received 2 June 1998)

The purpose of this paper is to study how the geometry and the spatial distribution of energy fluctuations of different length scales in a spiral vortex layer are related to each other in a time-dependent way. The numerical solution of Krasny [J. Comput. Phys. **65**, 292 (1986)], corresponding to the development of the Kelvin-Helmholtz instability, is analyzed in order to determine some geometrical features necessary for the analysis of Lundgren's unstrained spiral vortex. The energy distribution of the asymptotic solution of Lundgren characterized by a similar geometry is investigated analytically (1) in the wavelet radius-scale space, with a wavelet selective in the radial direction, and (2) in the wavelet azimuth-scale space, with a wavelet selective in the azimuthal direction. Energy in the wavelet radius-scale space is organized in ''blobs'' distributed in a way determined by the Kolmogorov capacity of the spiral $D_K \in [1,2]$ (which determines the rate of accumulation of spiral turns). As time evolves these blobs move towards the small scale region of the wavelet radius-scale space, until their scale is of the order of the diffusive length scale $\sqrt{\nu t}$, where $t$ is the time and $\nu$ is the kinematic viscosity. In contrast, energy in the wavelet azimuth-scale space is not localized, and is characterized by a shear-augmented viscous cutoff proportional to $\sqrt{\nu t^3}$. An accelerated viscous dissipation of the enstrophy and energy of Lundgren's spiral vortex is found for $D_K > 1.75$, but not for $D_K \leqslant 1.75$.
[S1063-651X(99)00605-4]

PACS number(s): 47.27.−i

## I. INTRODUCTION

Experimental as well as numerical analyses of the small scales of fully turbulent flows have shown that intense vorticity is organized into thin vortex tubes (see for example, Cadot, Douady, and Couder [1]; She, Jackson, and Orszag [2]; Ruetsch and Maxey [3]; Vincent and Meneguzzi [4]; Jiménez *et al.* [5]). These structures are remarkable in that their lifetime is relatively long, but their contribution to the spectrum of turbulence as well as their role in energy transfer and dissipation is still unknown. A complete understanding of the physical properties of these vortices requires an accurate knowledge of their structure. Different formation processes may lead to different structures. They may be formed following a Kelvin-Helmholtz instability [6,1,7,8], which is known to lead to spiral vortex layers likely to diffuse into a tubular filament. An asymptotic solution of such a spiral structure has been proposed by Lundgren [9] in the limit of long times. Another formation process, based on the destabilization of Burgers's strained vortex layer [10,11], has been proposed by Passot *et al.* [12] and also leads to vortex tubes.

Spiral vortices are barely observed in the small scales of turbulent flows (see, however, the experimental analyses of Cadot, Douady, and Couder [1] and Nicolleau and Vassilicos [13]). This might be due to insufficient resolution, but also to the fact that they are transient structures, as they diffuse into a vortex tube (Lundgren [9,8]), and that this process may be accelerated by the geometry of the spiral (Vassilicos [14], Flohr and Vassilicos [15], Angilella and Vassilicos [16]). One of the main effects of the winding up of a vortex layer is the generation locally in the flow of an entire range of length scales (Lundgren [9], Moffatt [17], Gilbert [18,19], Vassilicos and Hunt [20]), from the overall length scale of the structure to a minimal scale imposed by molecular diffusion.

The multiscale distribution of kinetic energy in a spiral vortex sheet is remarkable in that the scales involved are linked to specific positions within the structure, in a way determined by the geometry of the spiral. It is this geometrical link between position and scale that motivates the wavelet analysis we perform in Sec. III, as it enables us to unfold the distribution of energy in the wavelet position-scale space (Farge [21], Meneveau [22]).

To analyze the dynamical properties of a spiral vortex sheet we need to know its geometry. Several kinds of spirals exist in nature, such as the spiral of Archimedes [the equation of which is $r \sim \phi$ in polar coordinates $(r,\phi)$], the logarithmic spiral [$r \sim \exp(\alpha\phi)$], or the algebraic spiral ($r \sim \phi^{-\alpha}$, $\alpha > 0$). The Birkhoff-Rott equation, which governs the evolution of vortex sheets [6], has spiral vortex sheet solutions with a geometry depending on initial conditions. For example, it has a logarithmic spiral solution (Kambe [23]), with strength that diverges at infinity, and another solution in the form of a semi-infinite algebraic spiral vortex sheet (Kaden's spiral [6]). An efficient tool to determine the category of a spiral is the Kolmogorov capacity (fractal dimension). Indeed, it has been shown that among the three spirals quoted above (Archimedes, logarithmic, or algebraic) only the algebraic spiral has a nontrivial well-defined Kolmogorov capacity (Vassilicos and Hunt [20]). This means that when covering the algebraic spiral with boxes of size $l$, the minimal number $N(l)$ of boxes required to cover the structure satisfies

*Present address: LEMTA (CNRS UMR 7563), 2 Av. de la Forêt de Haye, 54504 Vandoeuvre, France.
†Author to whom correspondence should be addressed.

 

$$N(l) \simeq N(L)\left(\frac{l}{L}\right)^{-D_K} \quad \text{for } \eta \ll l \ll L, \tag{1}$$

where $D_K \in ]1,2[$ is the Kolmogorov capacity, $L$ is the overall length scale of the structure, and $\eta$ is the scale below which this power law is no longer satisfied. For example, fractals have a well-defined Kolmogorov capacity (see Falconer [24]). In the case of the algebraic spiral defined by $r \sim \phi^{-\alpha}$ we have (Vassilicos and Hunt [20])

$$D_K = 1 + \frac{1}{\alpha+1}. \tag{2}$$

Note that relation (2) is valid for a spiral with a relatively small number of resolved turns (see the Appendix of [20]).

In this paper we will apply this tool to a numerical solution of the Birkhoff-Rott equation corresponding to a double-branched spiral (Sec. II), in order to determine its geometry (logarithmic or algebraic). We will then investigate the time-dependent energy distribution in the vortex solution of Lundgren [9] (Sec. III) with a geometry similar to that determined in Sec. II, in both the wavelet radius-scale and wavelet azimuth-scale spaces. Finally, we will analyze the decay of enstrophy and energy of this vortex layer (Sec. IV). We now briefly present Lundgren's spiral vortex.

Lundgren [9] proposed a family of long-time asymptotic solutions of the Euler and Navier-Stokes equations involving spiral vortex sheets. In the case of inviscid fluids and for a two-dimensional double-branched spiral the asymptotic ($t \to +\infty$) solution reads

$$\omega(r,\phi,t) = 2\pi\gamma(r)[\delta(\phi - \Omega(r)t) + \delta(\phi - \pi - \Omega(r)t)], \tag{3}$$

where $\omega$ denotes vorticity, $\delta$ is a delta function, $\gamma(r)$ is the vorticity averaged over a circle of radius $r$, and $\Omega(r)$ is an angular frequency characteristic of a differential rotation. By writing that the flux of vorticity across a disk of radius $r$ equals the circulation along its perimeter we have (Lundgren [9])

$$4\pi r\gamma(r) = \frac{d}{dr}[2\pi r^2 \Omega(r)]. \tag{4}$$

This last relation manifests the fact that vorticity is not a passive scalar, but is the curl of velocity. Equation (3) is a long-time asymptotic solution of the vorticity equation provided $\Omega(r)$ is monotonically decreasing (see Lundgren [9]). One can check that the jump in tangential velocity across the vortex sheet is $2\pi\gamma(r)/[|\Omega'(r)|t]$ (Saffman [6], Pullin and Saffman [25]).

Following Lundgren [9] we expand the $\delta$ functions into Fourier modes to get

$$\omega(r,\phi,t) = 2\gamma(r) \sum_{n=-\infty}^{+\infty} e^{2in[\phi - \Omega(r)t]}. \tag{5}$$

Integration of Eq. (5) in the case where $\Omega(r) \sim r^{-1/\alpha}$ (following the method of Vassilicos and Brasseur [26]) shows that the radial component of velocity scales as $O(t^{-2})$, and that the azimuthal component reads

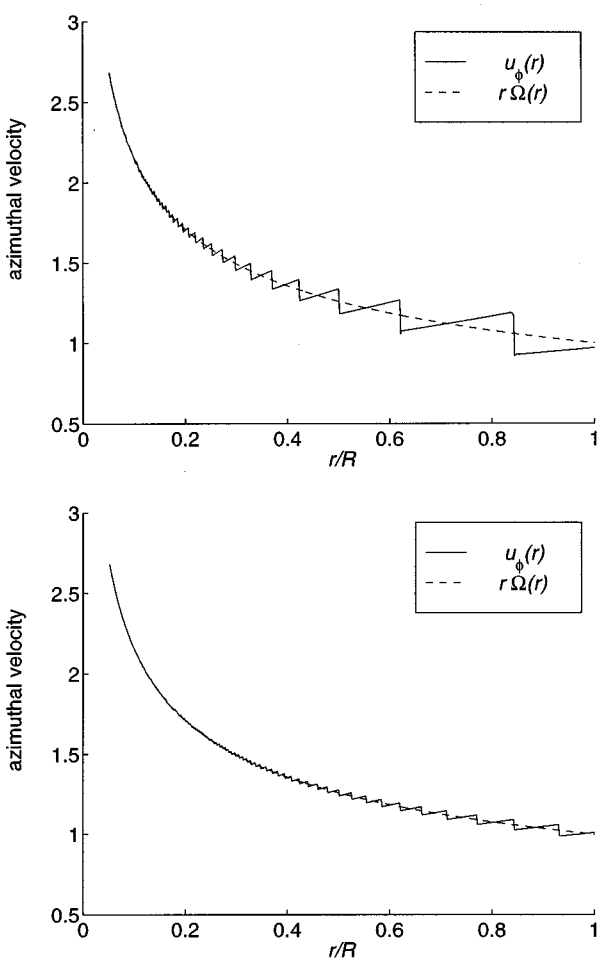


FIG. 1. One-dimensional cut through the azimuthal velocity field $u_\phi$ of Lundgren's spiral vortex sheet, plotted from Eqs. (6)–(8), for two different times $t_1$ and $t_2 > t_1$, and for an arbitrary decreasing angular frequency $\Omega(r)$. Velocity unit is $R\Omega(R)$. Discontinuities correspond to the position of the vortex sheet. The dashed line shows the azimuthal mode $n=0$ [i.e., $r\Omega(r)$]. As time advances, velocity jumps decrease, and will eventually vanish due to viscosity.

$$u_\phi(r,\phi,t) = \sum_{n=-\infty}^{+\infty} u_n(r,t) e^{2in\phi}, \tag{6}$$

with

$$u_0(r) = r\Omega(r) \tag{7}$$

and

$$u_n(r,t) = (2\alpha - 1)\frac{r}{t}\frac{1}{2in} e^{-2in\Omega(r)t} + O\left(\frac{1}{t^2}\right), \quad n \neq 0 \tag{8}$$

in the limit $t \to +\infty$. We therefore neglect the radial movement of the fluid in the limit $t \to +\infty$, so that the kinetic energy per unit mass is $\frac{1}{2}u_\phi^2$. This inviscid solution can easily be extended to the viscous case (see Sec. III). Figure 1 shows a plot of the azimuthal velocity $u_\phi(r,\phi,t)$ versus $r$ for two different times, obtained from Eqs. (6)–(8), and for an arbitrary decreasing angular frequency $\Omega(r)$ (300 azimuthal Fourier modes are used). As time advances, velocity jumps

(which can be thought of as velocity fluctuations) decrease and will eventually vanish due to viscosity.

At this stage it is important to focus our study with a specific choice of the angular velocity $\Omega(r)$. Indeed, the choice $\Omega(r)\sim r^{-1/\alpha}$ is arbitrary and has to be justified by means of experimental or numerical observations. To do this, we analyze in the next section a numerical solution of the Birkhoff-Rott equation corresponding to the development of the Kelvin-Helmholtz instability. This numerical solution is provided by the desingularization procedure of Krasny [27,28]. The choice of $\Omega(r)$ is important for two reasons. First, the mathematical calculation of the wavelet transform of the velocity relies heavily on the form of the phase of $u_n$, that is, $\Omega(r)t$. Secondly, the angular velocity determines some geometrical characteristics of the spiral, in particular its Kolmogorov capacity (fractal dimension), which, as discussed in Sec. IV, can seriously affect dissipative properties. A logarithmically decreasing $\Omega(r)$ leads to a logarithmic spiral, which is known to have a Kolmogorov capacity $D_K=1$ (Vassilicos and Hunt [20]). In contrast, if $\Omega(r)$ is a decreasing power law the corresponding spiral has a nonintegral Kolmogorov capacity.

## II. GEOMETRICAL PROPERTIES OF KRASNY'S SPIRAL VORTEX SHEET

A flat infinite vortex sheet of constant strength is known to be linearly unstable to infinitesimal two-dimensional disturbances (''Kelvin-Helmholtz'' instability). Moore [29] showed that the accumulation of vorticity at every second inflection point of sinusoidal perturbations leads to a singularity at a finite time $t_c$ of the order of $L/U$, where $U$ is the jump in tangential velocity of the vortex sheet and $L$ is the wavelength of the disturbance. By modifying the Birkhoff-Rott equations in such a way as to avoid the blow up of the strength of the sheet at $t=t_c$, Krasny [27,28] could compute an evolution of the sheet for $t>t_c$. This procedure is based on the introduction of a desingularization parameter $\delta$, such that the strength of the layer is bounded by a finite value which tends to $+\infty$ as $\delta\to 0$. For $t>t_c$ the vortex sheet rolls up around points where the strength is maximum, and takes the form of a spiral (see Fig. 2). The spiral obtained from this desingularization procedure is referred to as Krasny's spiral in this paper.

### A. Kolmogorov capacity

We have run a box-counting algorithm on the vortex sheet displayed in Fig. 2, obtained from Krasny's numerical procedure. Results are shown in Fig. 3, where the minimal number of boxes $N(l)$ required to cover the structure with boxes of size $l$ is plotted versus $l$. For short times ($t\simeq t_c$) we have $N(l)\sim l^{-1}$, so that $D_K=1$. During the roll-up process ($t>t_c$)$N(l)$ tends to a law of the form

$$N(l)\sim l^{-1.33},$$

corresponding to $D_K\approx 1.33$. This law holds for $Ut/L\geqslant 2.5$ and is valid over one decade of scales ($l/L\in[0.02,0.2]$). We conclude from Eq. (2) that $\alpha\approx 2$, in agreement with the measurements of Moffatt [30] operated on a one-dimensional cut through Krasny's spiral. Note that this result is in contradiction to the analysis of Everson and Sreenivasan [31], who concluded that Krasny's spiral is close to a logarithmic one.

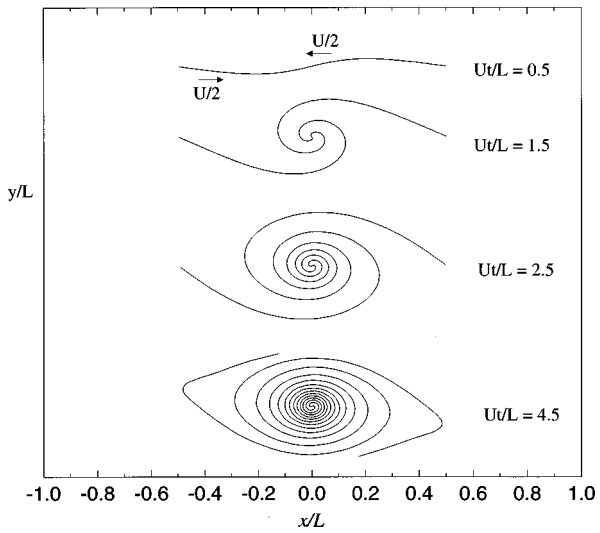


FIG. 2. Evolution of the interface between two adjacent streams using a desingularization procedure [27], for $t>t_c$. The desingularization parameter is $\delta/L=0.25$.

The fact that this spiral is of the form $r\sim\phi^{-\alpha}$ suggests that the roll up is due to a differential rotation of angular frequency $\Omega(r)\sim r^{-1/\alpha}$, so that the equation of the spiral might be approximated by

$$\phi=\Omega(r)t\sim r^{-1/\alpha}t. \tag{9}$$

In order to check that the points of the interface revolve around the center of the spiral with a well-defined angular frequency $\Omega(r)$ we have plotted the coordinates of an individual point versus time (Fig. 4). Clearly, for $t>L/U$ the point revolves around the center of the spiral [which is located at $(x,y)=(0,0)$] as its distance to the center does not vary significantly in time, in agreement with the fact that there is almost no radial movement. Note that the trajectory is in fact elliptic, and this effect might be due to the stretching induced by the periodic boundary conditions. The angu-

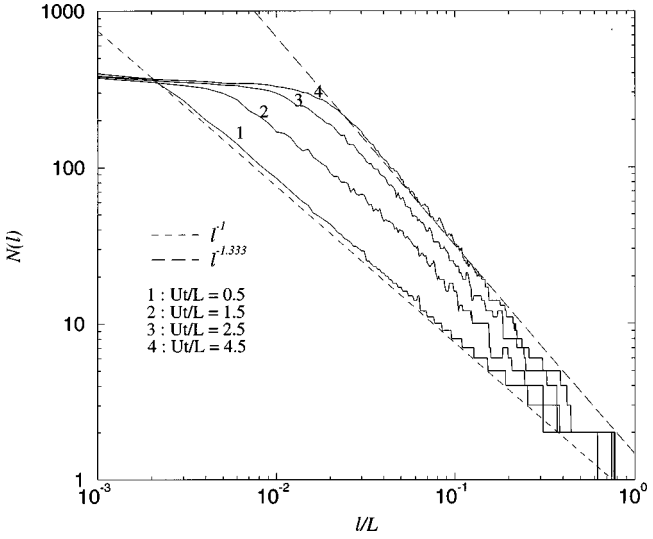


FIG. 3. Plot of the minimal number of boxes of size $l$ required to cover the vortex sheet of Fig. 2.

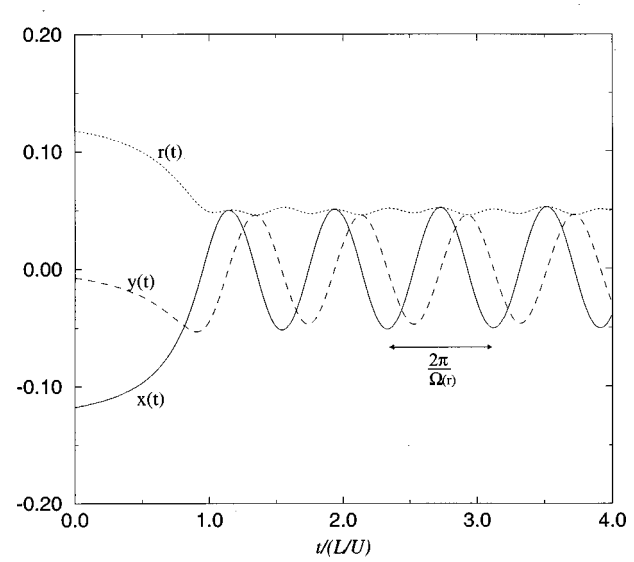


FIG. 4. Evolution of the Cartesian coordinates $(x,y)$ of a point of the interface displayed in Fig. 2. For $t>t_c$ the trajectory of the point is close to a circle of radius $r=(x^2+y^2)^{1/2}\simeq$const. The three length scales $x$, $y$, and $r$ are plotted in units of $L$.

lar frequency of such points can be measured, and Fig. 5 is a plot of $r^{1/2}\Omega(r)$ versus $r$ for a large number of points on the interface, at $t=4.5L/U$. It appears that in the range of radii $r/L\in[0.02,0.2]$ we have

$$\Omega(r)\simeq Cr^{-1/2}, \tag{10}$$

where $C\simeq 1.8UL^{-1/2}$. The exponent of this power law, together with the range of scales over which this law is valid, are in agreement with the estimation of $\alpha$ obtained from $N(l)$ (Fig. 3).

### B. Stretching of the spiral

In order to further check the validity of Eqs. (9) and (10) for Krasny's spiral, and in particular the time dependence of $\phi$, we calculate the total length of the layer predicted by such a roll-up process:

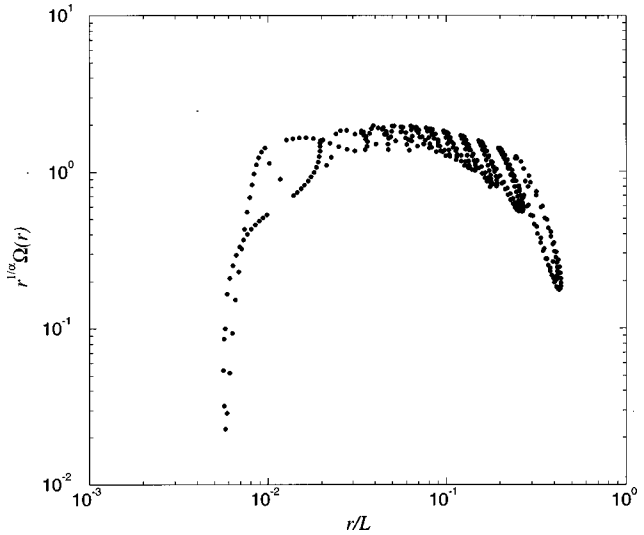


FIG. 5. Determination of the angular velocity $\Omega(r)$ (in units of $U/L$) of the points of the interface at $t=4.5L/U$. We have plotted $r^{1/\alpha}\Omega(r)$ with $\alpha=2$ (as suggested by the box-counting analysis).

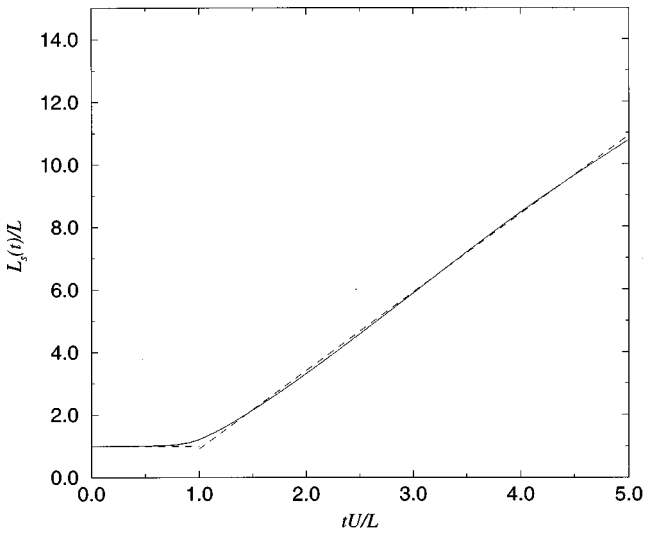


FIG. 6. Evolution of the length of the vortex sheet of Fig. 2 (solid line), together with predictions (12) and (13) (dashed lines).

$$L_s(t)=\int_{\text{spiral}} ds,$$

where $ds$ is the elementary arc length on the spiral:

$$ds^2=dr^2+(rd\phi)^2=dr^2\left[1+\left(rt\frac{d\Omega}{dr}\right)^2\right]. \tag{11}$$

In the limit $t\to 0$ we have $ds\simeq dr$ and

$$L_s(t)\simeq 2\int_0^{L/2} dr=L. \tag{12}$$

In the limit $t\to+\infty$ we have $ds\simeq rt|d\Omega/dr|dr$, and the total length of the spiral reads

$$L_s(t)\simeq 2t\int_0^{L/2}|d\Omega/dr|rdr,$$

and by making use of approximation (10) we get

$$L_s(t)\simeq L\times 2.5tU/L. \tag{13}$$

The time range for which the law (13) is valid is such that $rt|d\Omega/dr|\gg 1$ for all $r\in]0,L/2]$ [from Eq. (11)]. This condition is verified as soon as $t\gg(L/2)^{1/\alpha}\alpha/C$, that is, when $t\gg 0.8L/U$. Therefore, the transition between regimes (12) and (13) should occur at about one convective time $L/U$, which is also the order of the critical time $t_c$. Figure 6 shows $L_s(t)$ computed from the spiral of Fig. 2, together with predictions (12) and (13). These predictions are well verified, despite the fact that approximation (10) is not valid in the vicinity of the center of the spiral ($r/L<0.02$) and at the periphery of the spiral ($r/L>0.2$).

These results suggest that after vorticity concentrates at the inflection point and reaches a value prescribed by the desingularization parameter $\delta$, the sheet starts winding up into a spiral of the form $\phi=\Omega(r)t$, with $\Omega(r)$ given by Eq. (10).

### C. Choice of the angular frequency

The analysis of Krasny's spiral performed in this section suggests a power-law choice for the angular frequency $\Omega(r)$, i.e.,

$$\Omega(r)=\Omega_0\left(\frac{r}{R}\right)^{-1/\alpha}, \tag{14}$$

where $R$ is the radius of the overall structure and $\Omega_0$ is the angular frequency of points located at $r=R$. It also suggests that $\alpha\approx 2$, but we will not focus on this value in the remainder of this paper, and will more generally assume $\alpha>0$ (unless otherwise specified).

Note that the desingularization parameter used in the present work is of the order of the length scale $L$ of the initial disturbance ($\delta/L=0.25$), so that the desingularization procedure might influence the dynamics of the interface at those scales where we observe a well-defined Kolmogorov capacity (Fig. 3) corresponding to a power-law angular frequency (Fig. 5). Smaller values of $\delta$ lead to smaller spirals, i.e., spirals with an overall length scale of the order of $\delta$, with the same value of $D_K\simeq 1.33$ but in the approximative range $[0.1\delta,\delta]$ (see also Moffatt [30]). Therefore, the measures of $D_K$ and $\Omega(r)$ performed in this section will have to be interpreted with care. Future mathematical analyses of Krasny's desingularization procedure might enable us to clarify this point.

In the next section we study the time-dependent relation between spiral geometry and spatial distribution of energy fluctuations by operating a wavelet analysis on the velocity field $u_\phi(r,\phi,t)$ [Eqs. (6)–(8)] with $\Omega(r)$ given by Eq. (14).

## III. WAVELET ANALYSIS OF LUNDGREN'S SPIRAL VORTEX

In this section we perform a one-dimensional wavelet analysis on a radial cut through Lundgren's spiral vortex (''radial wavelet,'' Sec. III A), then on an azimuthal cut (''azimuthal wavelet,'' Sec. III B). We define the wavelet transform as follows. If $x$ denotes a spatial coordinate, the wavelet transform of a function $f(x)$ is

$$\tilde{f}(x,l)=\frac{1}{R}\int_{-\infty}^{+\infty} f(x')\,\theta\left(\frac{x'-x}{l}\right)dx', \tag{15}$$

where $\theta$ is the wavelet, $l$ is the scale of the wavelet, and the length scale $R$ is introduced for dimensional purposes. In the radial wavelet analysis $x$ denotes the radius $r$, and in the azimuthal wavelet analysis $x$ is the arc length $s$. The wavelet we choose is defined by

$$\theta(x)=\sin(mx)e^{-x^2/2}=\frac{e^{imx}-e^{-imx}}{2i}e^{-x^2/2}, \tag{16}$$

which is the imaginary part of the complex Morlet wavelet. By taking the imaginary part we ensure the condition

$$\int_{-\infty}^{+\infty}\theta(x)dx=0,$$

which is required for the wavelet transform to conserve energy, i.e.,

$$\int_0^{+\infty}\int_{-\infty}^{+\infty}|\tilde{f}(x,l)|^2\frac{dx}{x^2}dl=K\int_{-\infty}^{+\infty}|f(x)|^2dx,$$

with $K$ a finite constant (see, for example, Gasquet and Witomski [32], Farge [21], Hunt *et al.* [33]). The parameter $m$ in Eq. (16) is a constant which determines the number of oscillations of the wavelet. The moments of order $p>0$ of the wavelet are such that

$$\int_{-\infty}^{+\infty} r^p\,\theta(r)dr\sim m^p\exp(-m^2/2),$$

so that they can be set as small as desired by choosing $m$ large enough. We use this property of the Morlet wavelet in the calculation of the radial wavelet transform of $u_0$ (Appendix A). But our other motivation in choosing this wavelet is that it allows for the method of stationary phases to be conveniently applied, as we do below.

### A. Radial wavelet analysis

#### *1. Energy in the wavelet radius-scale space*

We start from Eq. (6). Using definition (15) the wavelet transform of $u_n(r,t)e^{2in\phi}$ (for a fixed azimuth $\phi$) reads

$$\tilde{u}_n(r,\phi,l)=\frac{1}{R}\int_0^R u_n(r',t)e^{2in\phi}\theta\left(\frac{r'-r}{l}\right)dr', \tag{17}$$

where $(r,\phi)$ are the polar coordinates of the position of the wavelet and $l$ is the wavelet scale parameter. In Eq. (17) the summation is not performed over $]-\infty,+\infty[$ because we have chosen to place the wavelet at radii $r\in[0,R]$ and to observe length scales $l$ such that $l\ll r$ and $l\ll R-r$ (see below), so that the summation can be reduced to the interval $[0,R]$. We show in Appendix A that the wavelet transform of $u_0=r\Omega(r)$ is negligible in the limit where $l\ll r$ and $l\ll R-r$. For $n\neq 0$, we insert expression (8) to get

$$\tilde{u}_n(r,\phi,l)\simeq\frac{1}{R}e^{2in\phi}\frac{2\alpha-1}{2int}\int_0^R r'e^{-2in\Omega(r')t}\theta\left(\frac{r'-r}{l}\right)dr'. \tag{18}$$

In Appendix B we calculate the above integral with the method of stationary phases, and obtain

$$\tilde{u}_n(r,\phi,l)\simeq A(1\pm i)\Omega_0 R(\Omega_0|n|t)^{-3/2}e^{2in\phi}\left(\frac{\bar{r}_{ltn}}{R}\right)^{2+1/2\alpha}\times e^{-(1/2)[(\bar{r}_{ltn}-r)/l]^2}e^{\pm i\psi(\bar{r}_{ltn})}, \tag{19}$$

in the limits $l\ll r$ and $l\ll R-r$, and $\Omega_0 t\gg 1$, where

$$\bar{r}_{ltn}=R\left(\frac{2|n|\Omega_0 tl}{\alpha mR}\right)^{\alpha/(\alpha+1)}, \tag{20}$$

and

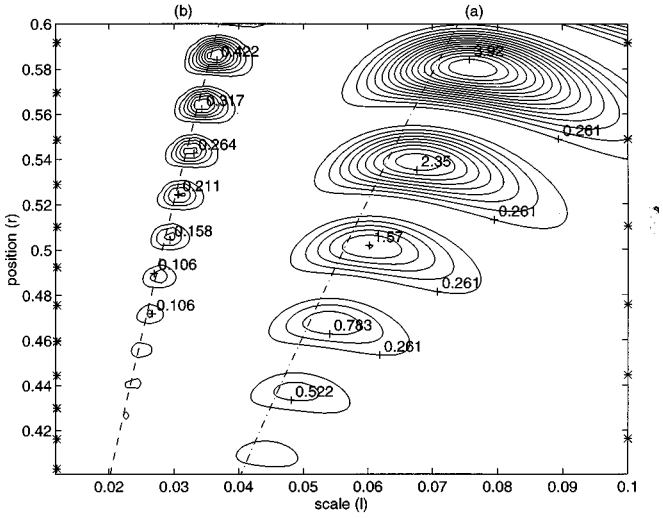


FIG. 7. Contour plot of the energy in the wavelet radius-scale space, from Eq. (23), for $\Omega_0 t=10\pi$ (a) and $\Omega_0 t=20\pi$ (b). The Kolmogorov capacity is $D_K=4/3$ ($\alpha=2$). The energy is organized in blobs located in the vicinity of the curve $l\sim\delta r$ (dashed line), where $\delta r$ is the distance between consecutive coils of the spiral at a distance $r$ from the center [Eq. (24)]. Stars on the left hand side indicate the position of the coils of the spiral at $\Omega_0 t=20\pi$, and stars on the right hand side indicate it at $\Omega_0 t=10\pi$. The accumulation point (center of the spiral) corresponds to $r=0$. As $t$ increases the blobs are closer to the curve $l\sim\delta r$. Both $r$ and $l$ are nondimensionalized by the radius of the spiral ($R$), and energy is nondimensionalized by $(\Omega_0 R)^2$.

$$A=\frac{2\alpha-1}{4\sqrt{2}}\sqrt{\pi}\left[\frac{1}{\alpha}\left(\frac{1}{\alpha}+1\right)\right]^{-1/2}$$

is a nondimensional real constant. The phase $\psi$ in Eq. (19) is defined in Eq. (B4) of Appendix B and is stationary in the vicinity of $\overline{r}_{ltn}$. Note that $\tilde{u}_n+\tilde{u}_{-n}$ is real, in agreement with the fact that both $u_\phi$ (6) and the wavelet (16) are real. We also deduce from Eq. (19) that the energy of the $\phi$-averaged $\tilde{u}_n$ scales as $|n|^{-(\alpha+4)/(\alpha+1)}$, so that as $\alpha\to 0$ ($D_K\to 2$) the mode $|n|=1$ contains the largest amount of energy. In the following we approximate the energy of $\tilde{u}_\phi(r,\phi,l)$ by taking into account only the mode $|n|=1$, and compare our analytical results with full numerical integration of $\tilde{u}_\phi(r,\phi,l)$.

By taking the half of the square of $\tilde{u}_1+\tilde{u}_{-1}$ and making use of Eq. (B1) we obtain the wavelet energy at position $(r,\phi)$ and scale $l$, in the limits $l\ll r$, $l\ll R-r$ and $\Omega_0 t\gg 1$:

$$e_{\text{inviscid}}(r,\phi,l)\simeq 2A^2(\Omega_0 R)^2(\Omega_0 t)^{-3}\left(\frac{\overline{r}_l}{R}\right)^{4+1/\alpha}\times\exp\left[-\left(\frac{\overline{r}_l-r}{l}\right)^2\right]\{1+\sin[4\phi-2\psi(\overline{r}_l)]\},\tag{21}$$

where $\overline{r}_l$ denotes $\overline{r}_{lt1}$ [Eq. (20)], that is,

$$\overline{r}_l=R\left(\frac{2\Omega_0 t l}{\alpha m R}\right)^{\alpha/(\alpha+1)}.\tag{22}$$

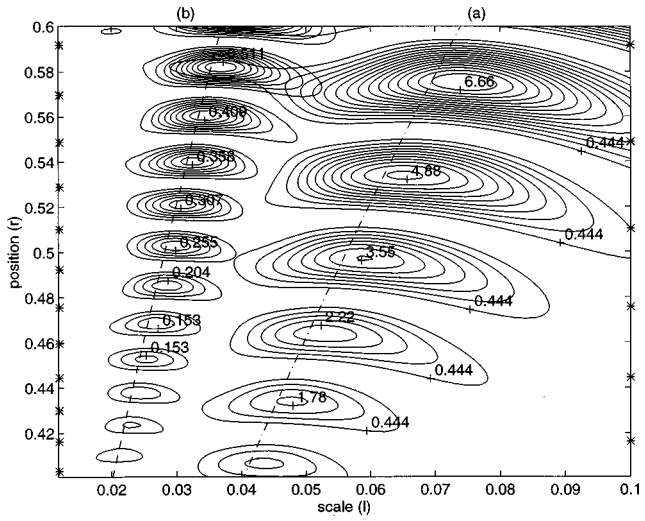


FIG. 8. Contour plot of the energy in the wavelet radius-scale space, obtained by computing 100 Fourier modes, and by taking into account the contribution of the velocity induced by the point vortex $[r\Omega(r)]$. Plot (a) corresponds to $\Omega_0 t=10\pi$ and plot (b) corresponds to $\Omega_0 t=20\pi$. The Kolmogorov capacity is $D_K=\frac{4}{3}$ ($\alpha=2$). Dashed lines correspond to the curve $l\sim\delta r$, where $\delta r$ is the distance between consecutive coils of the spiral at a distance $r$ from the center [Eq. (24)]. Notations and units are the same as in Fig. 7.

Finally, by making use of Eq. (22) the wavelet energy for $l\ll r$, $l\ll R-r$, $\Omega_0 t\gg 1$ in the inviscid case becomes

$$e_{\text{inviscid}}(r,\phi,l)\simeq B(\Omega_0 R)^2(\Omega_0 t)^{(\alpha-2)/(\alpha+1)}\left(\frac{l}{R}\right)^{(4\alpha+1)/(\alpha+1)}\times\exp\left[-\left(\frac{\overline{r}_l-r}{l}\right)^2\right]\{1+\sin[4\phi-2\psi(\overline{r}_l)]\},\tag{23}$$

where

$$B=2A^2\left(\frac{2}{\alpha m}\right)^{(4\alpha+1)/(\alpha+1)}$$

is a nondimensional constant.

We first notice from the exponential term in Eq. (23) that the kinetic energy is not distributed uniformly in the wavelet radius-scale space, and that the kinetic energy corresponding to a given scale $l$ is located in the vicinity of $(\overline{r}_l,l)$, where $\overline{r}_l$ is given by Eq. (22). Conversely, the kinetic energy corresponding to a given radius $r$ is located in the vicinity of the point $(r,\delta r)$ in the wavelet radius-scale space, where $\delta r$ is the distance between consecutive coils of the spiral at a distance $r$ from the center, that is (dropping constants of order unity),

$$\delta r\sim\frac{R}{\Omega_0 t}\left(\frac{r}{R}\right)^{1/\alpha+1}.\tag{24}$$

Figure 7 is a contour plot of the energy $e_{\text{inviscid}}(r,\phi,l)$ in the wavelet plane $(r,l)$ for two different times and for a fixed angle $\phi$, as obtained from Eq. (23). The Kolmogorov capacity is $D_K=4/3$ ($\alpha=2$). For comparison, Fig. 8 shows the

energy obtained from a numerical computation of the wavelet transform of Eq. (6), with 100 azimuthal Fourier modes, including the mode $n=0$ [that is, $r\Omega(r)$]. The energy is organized in ''blobs'' which are asymptotically centered on the curve $l\sim\delta r$. Changing the azimuth $\phi$ makes the blobs shift along the curve $l\sim\delta r$, but does not change the overall distribution of the blobs. This is an effect of the term $\sin[4\phi-2\psi(\overline{r_l})]$ in Eq. (23) which determines the periodicity of the blobs along the curve $l\sim\delta r$.

The energy $e_{\text{inviscid}}(r,l)$ corresponds to velocity fluctuations of length scale $l$ at a distance $r$ from the center of the spiral, and Eq. (23) shows that these fluctuations are localized in the sense that $l\sim\delta r(t)$, where $\delta r(t)$ is the distance between the consecutive coils of the spiral at that $r$ [Eq. (24)]. Keeping $r$ fixed, the distance $\delta r(t)$ between consecutive coils decreases with time [Eq. (24)] because of the spiral's differential rotation. Also, the velocity fluctuation at this radius decreases as $1/t$, and the combination of these two effects leads to a decay of the energy at $(r,\delta(r))$ of the form $e_{\text{inviscid}}(r,\delta(r))\sim t^{-3}$ [from Eq. (23)]. Keeping $l$ fixed, the wavelet energy of length scale $l$ moves outwards in space as it is localized around $\overline{r_l}\sim t^{\alpha/(\alpha+1)}$ [from Eq. (22)]. In the wavelet radius-scale space this transfer mechanism is illustrated by the movement and distortion of the curve $l\sim\delta r$ towards the $l=0$ axis as time advances (see Figs. 7 and 8). In real fluids this mechanism is broken by viscous dissipation.

Clearly, the structure of kinetic energy in the wavelet radius-scale space reflects the complex spatial structure of the Lundgren spiral. Such a structure could not be found in a Fourier analysis, since the Fourier spectrum contains no spatial information. Indeed, the Fourier spectrum of a one-dimensional cut of velocity along the azimuth $\phi$ can be obtained by integrating the kinetic energy $e_{\text{inviscid}}(r,\phi,l)$ over all radii $r$. [This is not exactly the Fourier spectrum, as it contains terms involving the wavelet. Nevertheless, it can be thought of as the Fourier spectrum ''smoothed'' by the wavelet (see, for example, Farge [21]).] One can easily check from Eq. (23) that this $r$ integration would make the exponential term $\exp\{-[(\overline{r_l}-r)/l]^2\}$ and the sine term vanish (these two terms are responsible for the structure of $e_{\text{inviscid}}$). Indeed, $e_{\text{inviscid}}$ is of the form

$$e_{\text{inviscid}}(r,\phi,l)\simeq F(t)l^{(4\alpha+1)/(\alpha+1)}G_\phi\left(\frac{\overline{r_l}-r}{l}\right),$$

with $G_\phi$ localized around 0. Hence,

$$\begin{aligned}e_{\text{inviscid}}(l,\phi)&\equiv\int_0^R e_{\text{inviscid}}(r,\phi,l)\,dr\\&\simeq l^{(4\alpha+1)/(\alpha+1)+1}\int_{(\overline{r_l}-R)/l}^{\overline{r_l}/l}G_\phi(y)\,dy\\&\sim l^{(4\alpha+1)/(\alpha+1)+1},\end{aligned}$$

because $-(\overline{r_l}-R)/l\gg1$ and $\overline{r_l}/l\gg1$ and $G_\phi$ is localized around 0. Therefore, the resulting ''Fourier'' spectrum has no structure (it is only a power law of $l$) and both the spatial information and the scale information are necessary to observe these blobs.

In the next section we generalize the calculation of the wavelet radius-scale energy (23) to the viscous case and discuss the effect of viscosity.

#### *2. Viscous cutoff in the radial direction*

The effect of the viscous diffusion of the coils of the spiral is that the reduction of the scales, and therefore the displacement of the blobs of energy in the wavelet radius-scale space, will eventually stop and the energy carried out by the blobs will then be transformed into heat. In order to investigate this effect we generalize expression (23) to the viscous case. We start from the asymptotic ($t\to+\infty$) solution of the viscous vorticity equation (Lundgren [9])

$$\omega(r,\phi,t)\simeq2\gamma(r)\sum_{n=-\infty}^{+\infty}e^{2in[\phi-\Omega(r)t]}e^{-(4/3)n^2\Omega'^2\nu t^3},\tag{25}$$

which corresponds to the double-branched inviscid spiral solution (3)–(5) in the limit $\nu\to0$. In particular, $\gamma(r)$ and $\Omega(r)$ are still related by the kinematic relation (4).

As pointed out by Lundgren [9], the exponential term in Eq. (25) enables us to calculate the radius $\rho(t)$ below which all the modes are damped by viscosity, and $\rho(t)$ can be thought of as the radius below which the spiral structure has been smoothed out and no longer exists:

$$\rho(t)=R\left(\frac{\Omega_0\sqrt{\nu t^3}}{R}\right)^{\alpha/(\alpha+1)}=R\left(\frac{\Omega_0\sqrt{\nu t^3}}{R}\right)^{2-D_K}.\tag{26}$$

By integrating Eq. (25) in the way performed for the inviscid case by Vassilicos and Brasseur [26] we get

$$u_\phi(r,\phi,t)=\sum_{n=-\infty}^{+\infty}u_n(r,t)e^{2in\phi},\tag{27}$$

with

$$u_0(r)=r\Omega(r)$$

and

$$\begin{aligned}u_n(r,t)=(2\alpha-1)\frac{r}{t}\frac{1}{2in}e^{-in\Omega(r)t}\left[1+O\left(\frac{n^2\Omega'^2(r)\nu t^3}{n\Omega(r)t}\right)\right]\\\times e^{-(4/3)n^2\Omega'^2\nu t^3},\quad n\neq0\end{aligned}\tag{28}$$

in the limit $t\to+\infty$. Because $n\Omega(r)t\gg1$, a sufficient condition for the order term ($O$) in Eq. (28) to be negligible is $n^2\Omega'^2\nu t^3<1$. Therefore, expression (28) is valid everywhere outside the inviscid core of the spiral [i.e., for all $r\gg\rho(t)$].

Under this condition the energy in the wavelet radius-scale space can be readily calculated by means of the method of stationary phases, and reads

$$e(r,\phi,l)=e_{\text{inviscid}}(r,\phi,l)\exp\left(-\frac{2}{3}m^2\frac{\nu t}{l^2}\right).\tag{29}$$

We therefore observe that viscosity is responsible for a cutoff $\sqrt{\nu t}$ in the wavelet radius-scale space, because the energy $e(r,\phi,l)$ is negligible for any $r$ and $\phi$ where $l\ll\sqrt{\nu t}$, and

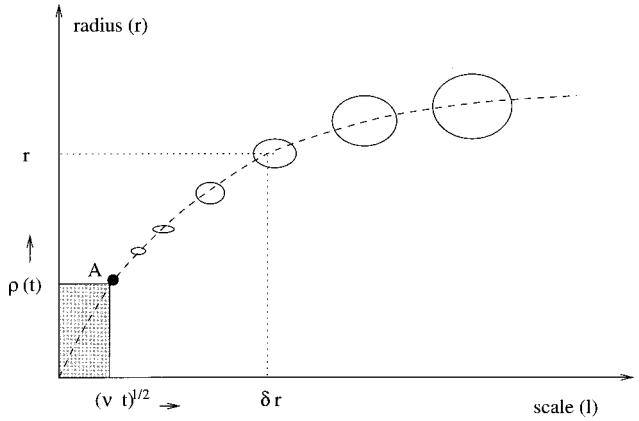


FIG. 9. Sketch of the blobs of kinetic energy in the wavelet radius-scale space $(r,l)$, at a fixed time $t$. The gray area defined by $r<\rho(t)$ and $l<(\nu t)^{1/2}$ is the image of the inviscid core of the spiral in the wavelet radius-scale space. Most of the energy dissipation occurs in the vicinity of the point $A(t)=(\rho(t),(\nu t)^{1/2})$.

where $l\gg\sqrt{\nu t}$ we have $e(r,\phi,l)\simeq e_{\text{inviscid}}(r,\phi,l)$. This means that energy transfers occurring at a position $r$ as a result of the spiral vortex sheet's differential rotation stop when the intercoil distance $\delta r$ [Eq. (24)] is of the order of the radial diffusive length scale $\sqrt{\nu t}$. This is in agreement with Moore and Saffman [34], who noticed that the coils of the spiral are thickened by viscous diffusion, so that the discrete jumps in the flow field are replaced by smoothed out gradients of thickness $\sqrt{\nu t}$ (Moore and Saffman [34]). The position of the coil where $\delta r\sim\sqrt{\nu t}$ is given by $r\sim\overline{r_l}$ with $l=\sqrt{\nu t}$, that is, $r\sim\rho(t)$. Hence, the ''image'' of the viscous core in the wavelet radius-scale space is the region defined by

$$r<\rho(t)$$

and

$$l<\sqrt{\nu t}.$$

Figure 9 shows a sketch of this region, together with blobs of energy located on the curve $l\sim\delta r$. Energy dissipation occurs only in the vicinity of the point $A=(\rho(t),\sqrt{\nu t})$. Indeed, there is no dissipation in the area $\{r\ll\rho(t)$ and $l\ll\sqrt{\nu t}\}$ because gradients have been smoothed out in the core, and there is no dissipation in the area $\{r\gg\rho(t)$ or $l\gg\sqrt{\nu t}\}$ because viscous effects are negligible there [Eq. (29)].

### B. Azimuthal wavelet analysis

The radial wavelet analysis of the preceding section is an analysis of the effect of the differential rotation on the radial distribution of energy. In order to investigate the effect of the differential rotation on the azimuthal distribution of energy, we perform a wavelet analysis similar to the one of Sec. III A, but with a wavelet selective in the azimuthal direction. For a fixed radius $r$ we calculate the wavelet transform of $u(r,\phi)$ as defined in Eq. (15), but by integrating over the domain $s\in[r(\phi-\pi),r(\phi+\pi)]$ instead of $x\in]-\infty,+\infty[$:

$$\tilde{u}(r,\phi,l)=\frac{1}{R}\int_{r(\phi-\pi)}^{r(\phi+\pi)}\theta\left(\frac{s'-s}{l}\right)u(r,\phi')ds', \qquad (30)$$

where the arc lengths $s$ and $s'$ are such that $s'-s=r(\phi'-\phi)$ and $ds'=rd\phi'$. Integration is performed over the circle of radius $r$ centered at the origin. For all $n$ the wavelet transform of the mode $e^{2in\phi}u_n(r)$ is

$$\tilde{u}_n(r,\phi,l)=u_n(r,t)\frac{r}{R}\int_{\phi-\pi}^{\phi+\pi}\theta\left(r\frac{\phi'-\phi}{l}\right)e^{2in\phi'}d\phi'.$$

By performing the change of variables $y=r/l(\phi'-\phi)$ we get

$$\tilde{u}_n(r,\phi,l)=\frac{l}{R}e^{2in\phi}u_n(r,t)\int_{-\pi r/l}^{\pi r/l}e^{i(2nl/r-m)y}e^{-(1/2)y^2}dy.$$

In the limit where $r\gg l$ the above integral is increasingly well approximated by

$$\int_{-\infty}^{\infty}e^{i(2nl/r-m)y}e^{-(1/2)y^2}dy=(\pi/2)^{1/2}\exp[-\tfrac{1}{2}(2nl/r-m)^2],$$

so that

$$\tilde{u}_n(r,\phi,l)\simeq(\pi/2)^{1/2}\frac{l}{R}e^{2in\phi}u_n(r,t)\exp\left[-\frac{r}{l}\left(n-\frac{rm}{2l}\right)^2\right]. \qquad (31)$$

In contrast with the radial wavelet analysis the azimuthal wavelet transform of the first azimuthal mode ($|n|=1$) does not dominate over the other azimuthal modes. It is the mode $\overline{n}\sim rm/(2l)$ which carries the largest contribution in $\tilde{u}(r,\phi,l)=\Sigma_n\tilde{u}_n(r,\phi,l)$, and as $r\gg l$ the contribution of other modes is exponentially small. We therefore approximate the wavelet transform of $u(r,\phi,l)$ by

$$\tilde{u}(r,\phi,l)\simeq\tilde{u}_{\overline{n}}(r,\phi,t)+\tilde{u}_{-\overline{n}}(r,\phi,t).$$

By taking the half of the square of $\tilde{u}(r,\phi,l)$ we obtain the energy in the wavelet azimuth-scale space

$$e(r,\phi,l)\simeq\pi(2\alpha-1)^2\left(\frac{l^2}{mRt}\right)^2\sin^2\left(\frac{mr}{l}[\phi-\Omega(r)t]\right)\times\exp\left[-\frac{2}{3}\left(\frac{mr}{l}\right)^2\Omega'^2(r)\nu t^3\right], \qquad (32)$$

for $l\ll r$. We first observe that the exponential drop off in Eq. (32) represents the cutoff induced by viscosity, and that the energy has therefore been mostly dissipated at the length scales $l$ such that

$$\left(\frac{mr}{l}\right)^2\Omega'^2(r)\nu t^3\gg 1,$$

that is,

$$l\ll\Omega(r)t\sqrt{\nu t}.$$

The viscous length scale $\Omega(r)t\sqrt{\nu t}$ drops out quite naturally from this azimuthal wavelet analysis. It depends on the radius $r$ and is much larger than $\sqrt{\nu t}$ because of the shear induced by the differential rotation (Rhines and Young [35], Flohr and Vassilicos [15]). Hence, the viscous diffusion is shear augmented in the azimuthal direction, and this effect is proportional to the local strain rate $\Omega(r)$.

For scales much larger than the viscous cutoff length scale $\Omega(r)t\sqrt{\nu t}$ we observe that the energy (32) is not localized in the wavelet azimuth-scale space, in contrast with the wavelet radius-scale analysis. Indeed, for $l \gg \Omega(r)t\sqrt{\nu t}$ we can drop the exponential viscous term in Eq. (32), and the remaining term is a combination of a power function and of a sine function of $\phi$ and $l$ which displays activity everywhere in the $(\phi,l)$ space. This significant difference between the wavelet radius-scale and the wavelet azimuth-scale wavelet analyses enables us to draw interesting conclusions as to the distribution of energy in the spiral vortex.

### C. Characteristic scales of energy distribution

The energy distribution in the wavelet radius-scale space is localized (Sec. III A). In contrast, the energy distribution in the wavelet azimuth-scale space is not localized, as it displays activity everywhere in this space (Sec. III B). This suggests that between two coils located at radii $r$ and $r+\delta r$, the typical scale of velocity fluctuations is $\delta r$ rather than the perimeter $2\pi r$.

For a fixed radius $r$ the intercoil distance $\delta r$ decreases as the vortex sheet rolls up [see Eq. (24)], so that the energy of fluctuations is distributed on smaller and smaller scales. The distribution of energy in the wavelet radius-scale space therefore changes, and we calculate its rate of change $\partial e/\partial t$ from Eqs. (29) and (23). For a given scale $l$ we consider the energy at the coil of radius $\overline{r_l}$. We then calculate the rate of change of $e(\overline{r_l},\phi,l)$ from results (29) and (23). By noticing that

$$\frac{\partial \psi(\overline{r_l})}{\partial t} = 2\Omega(\overline{r_l}),$$

and focusing where $r=\overline{r_l}$, we are led to

$$\frac{\partial e}{\partial t}(\overline{r_l},\phi,l) \simeq \overline{e}(l)\left[4\Omega(\overline{r_l})C(r,\phi) - \frac{2}{3}m^2\frac{\nu}{l^2}S(r,\phi)\right] + O((\Omega_0 t)^{-3/(\alpha+1)}), \tag{33}$$

where

$$C(r,\phi) = \cos[4\phi - 2\psi(\overline{r_l})], \tag{34}$$

$$S(r,\phi) = 1 - \sin[4\phi - 2\psi(\overline{r_l})], \tag{35}$$

and

$$\overline{e}(l) = B^2(\Omega_0 R)^2(\Omega_0 t)^{(\alpha-2)/(\alpha+1)}\left(\frac{l}{R}\right)^{(4\alpha+1)/(\alpha+1)} \times \exp\left(-\frac{2}{3}m^2\frac{\nu t}{l^2}\right)$$

is the maximum energy of a given scale $l$. From Eq. (33) we deduce that the energy transfer at scale $l$ and position $\overline{r_l}$ has two different regimes, according to whether the ratio

$$\mathrm{Re}(l) = \frac{l^2\Omega(\overline{r_l})}{\nu} \tag{36}$$

is large or not. Re($l$) plays the role of a local Reynolds number, and indicates whether the scale $l$ is inviscid or not. Re($l$) is the ratio of the diffusive time needed to smooth out the intercoil distance $l$, namely, $l^2/\nu$, to the corresponding circumferential convective time $\Omega(\overline{r_l})^{-1}$. When Re($l$)$\gg$1 the characteristic time of energy variations at scale $l$ is the circumferential convective time (turnover time). Note that this time is also $l/u$, where $l=\delta r$ is the characteristic scale of velocity fluctuations, and $u \sim r/t$ is the typical value of velocity fluctuations at radius $r$ (see Introduction). Note also that results should differ in the case of a three-dimensional strained spiral vortex layer.

The analysis of $\partial e/\partial t$ shows that, at a distance $r$ from the center, energy is transferred from the scale $\delta r$ to other scales over a turnover time $\Omega(r)^{-1}$. However, this energy transfer can also be thought of in terms of *scale displacement* in the wavelet radius-scale space. Indeed, a given scale $l$ is associated with a position $\overline{r_l}$. Because this radius increases with $t$ [Eq. (22)] the scale $l$ moves outwards in the physical space towards the periphery of the spiral. We can define the speed of the scale $l$ by $\partial\overline{r_l}/\partial t$, that is,

$$\frac{\partial\overline{r_l}}{\partial t} = \frac{2}{m(\alpha+1)}l\Omega(\overline{r_l}),$$

and a typical duration of the scale movement is

$$\frac{l}{\partial\overline{r_l}/\partial t} \sim \frac{1}{\Omega(\overline{r_l})},$$

which is the convective time around the coil of radius $\overline{r_l}$, and has also been found to be the characteristic time of energy transfer of scale $l$.

## IV. ENSTROPHY AND ENERGY DECAY OF LUNDGREN'S SPIRAL VORTEX

The enstrophy decay depends on two different mechanisms (Flohr and Vassilicos [15]). First, the shear induced by the differential rotation accelerates the diffusion, as it sharpens the gradients of the vorticity field. Second, the spiral structure resulting from the roll up is likely to have anomalous diffusive properties (Vassilicos [14], Flohr and Vassilicos [15], Angilella and Vassilicos [16]). In this section we calculate the enstrophy of the structure in order to analyze these effects. We integrate the squared vorticity within an annular area $\{r_0 \leqslant r \leqslant R\}$:

$$\langle\omega^2\rangle = \frac{1}{\pi R^2}\int_{r_0}^{R}\left(\int \omega^2(r,\phi,t)\,d\phi\right) r\,dr, \tag{37}$$

where $r_0$ is a small radial scale chosen such that $r_0 \ll \rho(t)$ and $R$ is the overall length scale of the structure. Because of the absence of radial movement there is no flux of vorticity through the boundaries of the domain $\{r_0 \leqslant r \leqslant R\}$. Follow-

ing Lundgren [9], we calculate the $\phi$ integral in Eq. (37) by using the Fourier series in $\phi$ of $\omega$ [Eq. (25)], and applying the Plancherel identity. Equation (37) becomes

$$\langle\omega^2\rangle \simeq \frac{2}{R^2}\sum_{n=0}^{+\infty}\int_{r_0}^{R} 4\gamma(r)^2 e^{-(8/3)n^2\Omega'^2\nu t^3} r\,dr. \quad (38)$$

The vortex strength $\gamma(r)$ is linked to the angular frequency by Eq. (4), and reads

$$\gamma(r)=\frac{1}{2}\left(2-\frac{1}{\alpha}\right)\Omega_0(r/R)^{-(1/\alpha)}. \quad (39)$$

In Eq. (38) the contribution of the mode $n=0$ can be readily calculated and is a constant depending only on the parameters $\Omega_0$, $\alpha$, $R$, and $r_0$. We focus on the contribution of the modes $n>0$ which is calculated by making use of the change of variables

$$X=n^2\Omega'^2(r)\nu t^3=n^2(\Omega_0 R^{1/\alpha})^2\frac{1}{\alpha^2}r^{-2/\alpha-2}\nu t^3, \quad (40)$$

$$r=\left(\frac{X}{n^2(\Omega_0 R^{1/\alpha})^2(1/\alpha^2)\nu t^3}\right)^{-1/(2/\alpha+2)}, \quad (41)$$

and reads

$$\begin{aligned}\langle\omega^2\rangle \simeq{}& \frac{(2\alpha-1)^2}{\alpha(1+\alpha)}\left(\frac{1}{\alpha^2}\right)^{(\alpha-1)/(\alpha+1)}\\ &\times\Omega_0^2(\Omega_0^2R^{-2}\nu t^3)^{(\alpha-1)/(\alpha+1)}\\ &\times\sum_n n^{2(\alpha-1)/(\alpha+1)}\int_{n^2\Omega'^2(R)\nu t^3}^{n^2\Omega'^2(r_0)\nu t^3}\\ &\times e^{-8X/3}X^{-2\alpha/(\alpha+1)}dX. \end{aligned} \quad (42)$$

We now perform time asymptotics by noticing that the above integral reads

$$\begin{aligned}&\int_{n^2\Omega'^2(R)\nu t^3}^{n^2\Omega'^2(r_0)\nu t^3} e^{-8X/3}X^{-2\alpha/(\alpha+1)}dX\\ &=\left(\frac{8}{3}\right)^{(\alpha-1)/(\alpha+1)}\left[\Gamma\left(\frac{\alpha-1}{\alpha+1},\frac{8}{3}n^2\Omega'^2(R)\nu t^3\right)\right.\\ &\left.-\Gamma\left(\frac{\alpha-1}{\alpha+1},\frac{8}{3}n^2\Omega'^2(r_0)\nu t^3\right)\right],\end{aligned}$$

where $\Gamma(\cdots)$ denotes the incomplete gamma function (see [36]). These two gamma functions are exponentially small as soon as $n^2\Omega'^2(R)\nu t^3\gg 1$, that is,

$$n\gg N=\frac{\alpha R}{\Omega_0\sqrt{\nu t^3}} \quad (43)$$

(see also Flohr and Vassilicos [15]). This enables us to truncate the series in Eq. (42), so that summation is now restricted to indices $1\leqslant n\leqslant N$. For these indices the first gamma function is constant at leading order, and equal to $\Gamma((\alpha-1)/(\alpha+1))$, and the second one is exponentially small because $r_0\ll\rho(t)$ implies that for all $n>0$ we have $n^2\Omega'^2(r_0)\nu t^3\gg 1$. Finally enstrophy reads

$$\langle\omega^2\rangle\simeq C_1\Omega_0^2(\Omega_0^2R^{-2}\nu t^3)^{(\alpha-1)/(\alpha+1)}\sum_{1\leqslant n\leqslant N} n^{2(\alpha-1)/(\alpha+1)}, \quad (44)$$

where

$$C_1=\frac{(2\alpha-1)^2}{\alpha(1+\alpha)}\left(\frac{8}{3\alpha^2}\right)^{(\alpha-1)/(\alpha+1)}\Gamma\left(\frac{\alpha-1}{\alpha+1}\right)$$

is a constant of order unity which only depends on the geometry of the spiral. At this stage we notice that if $N\gg 1$, i.e., $\Omega_0(\alpha R)^{-1}\sqrt{\nu t^3}\ll 1$, the sum in Eq. (44) can be approximated by $|1-N^{(3\alpha-1)/(\alpha+1)}|$. For $\alpha<\frac{1}{3}$ this term is constant at leading order, and we get

$$\langle\omega^2\rangle\sim\Omega_0^2\left(\frac{\Omega_0 t}{\mathrm{Re}^{1/3}}\right)^{3(3-2D_K)}$$

$$\text{for } 1\ll\Omega_0 t\ll\mathrm{Re}^{1/3} \text{ and } D_K>1.75, \quad (45)$$

where we have made use of relation (2) and introduced the Reynolds number based on the circumferential velocity $\Omega_0 R$ and the radius $R$ (see also Flohr and Vassilicos [15]):

$$\mathrm{Re}=\frac{R^2\Omega_0}{\nu}. \quad (46)$$

For $\alpha>1/3(D_K<1.75)$ we have $|1-N^{(3\alpha-1)/(\alpha+1)}|\simeq N^{(3\alpha-1)/(\alpha+1)}$, and by making use of Eq. (43) we obtain

$$\langle\omega^2\rangle\sim\Omega_0^2\left(\frac{\Omega_0 t}{\mathrm{Re}^{1/3}}\right)^{-3/2} \quad \text{for } 1\ll\Omega_0 t\ll\mathrm{Re}^{1/3} \text{ and } D_K\leqslant 1.75. \quad (47)$$

The energy $E(t)$ of velocity fluctuations can be calculated similarly by integrating the modes $n\neq 0$ in the Fourier representation of $u(r,\phi,t)$ [Eqs. (27) and (28)], and reads

$$E(t)\sim(R\Omega_0)^2\,\mathrm{Re}^{-2/3}\left(\frac{\Omega_0 t}{\mathrm{Re}^{1/3}}\right)^{2(5-3D_K)}$$

$$\text{for } 1\ll\Omega_0 t\ll\mathrm{Re}^{1/3} \text{ and } D_K>1.75, \quad (48)$$

$$E(t)\sim(R\Omega_0)^2\,\mathrm{Re}^{-2.3}\left(\frac{\Omega_0 t}{\mathrm{Re}^{1/3}}\right)^{-1/2}$$

$$\text{for } 1\ll\Omega_0 t\ll\mathrm{Re}^{1/3} \text{ and } D_K\leqslant 1.75. \quad (49)$$

Results (45) and (48) show that for $D_K>1.75$ the decay of enstrophy and energy is accelerated by the space-filling property of the spiral (see Vassilicos [14], Flohr and Vassilicos [15]), whereas results (47) and (49) show that for $D_K\leqslant 1.75$ the decay is not sensitive to this space-filling property. This is to be linked with the fact that the energy spectrum of Lundgren's vortex scales as $k^{-2}$ at large wave number $k$ for all $D_K\leqslant 1.75$ (Lundgren [9], Gilbert [18,19]), but scales as $k^{4D_K-9}$ for $D_K>1.75$ (see Malik and Vassilicos [37], and Appendix C of this paper). Therefore, for $D_K>1.75$, the larger the $D_K$ the more singular the vorticity and

velocity fields, and the more sensitive they are to viscous dissipation. A similar behavior has been observed for rolled-up vortex *patches* (Gilbert [18]), as the power of the spectrum of the velocity induced by a rolled-up vortex patch is observed to depend on $D_K$ for $D_K>1.5$, and to be independent of $D_K$ for $D_K<1.5$. As noticed by Gilbert [18], a spiral vortex patch with $D_K<1.5$ is too ''weak'' a singularity to induce an energy spectrum different from that of an isolated discontinuity. Similarly, in the case of the vortex sheet investigated in this paper we observe anomalous diffusive properties only for $D_K>1.75$.

One can also check from Eq. (48) [or similarly from Eq. (45)] that the rate of energy decay $dE(t)/dt$ is such that

$$\frac{dE(t)}{dt}\sim \mathrm{Re}^{2(D_K-2)},$$

so that it is asymptotically independent of Re in the limit where $D_K\to 2$ (i.e., $\alpha\to 0$). This result could be linked to the fact that the dissipation rate of kinetic energy in turbulent flows is independent of the viscosity $\nu$ when $\nu\to 0$. Nevertheless, the problem of turbulence is exceedingly complex, and the properties of the dissipation rate of energy in turbulent flow cannot be reduced without care to the properties of a single vortical structure. Further analyses, like topological analyses of dissipative zones in turbulent flows, could be useful to investigate this point.

Note that a similar result has also been observed by Flohr and Vassilicos [15] about the rate of decay of the variance of a scalar patch wrapped around a vortex.

## V. CONCLUSION

We have investigated the distribution of energy in a rolled-up vortex layer by making use of the asymptotic spiral vortex model of Lundgren [9], in the unstrained case.

In order to choose the angular frequency $\Omega(r)$ in Lundgren's model we have investigated some geometrical properties of a numerical solution of the Birkhoff-Rott equation (Krasny [27,28]) corresponding to a rolled-up vortex sheet. This solution is observed to be close to an algebraic, rather than logarithmic (Kambe [23]), spiral. This observation is in agreement with the one-dimensional measurements of Moffatt [30], and in contradiction to the analysis of Everson and Sreenivasan [31]. The Kolmogorov capacity of Krasny's spiral has been measured and is found to be close to $D_K=1.33$. This suggests that the equation of the spiral can be approximated by $\phi=\Omega(r)t$ for times much longer than the critical time of the vortex sheet $L/U$, with $\Omega(r)\sim r^{-1/2}$. This approximation implies that the length of the vortex sheet increases like $t$ for $t>L/U$, and this prediction has also been verified for Krasny's spiral.

However, the ratio of the desingularization parameter $\delta$ to the overall length scale of the spiral being of order 1, these conclusions have to be taken with care, as the desingularization procedure might influence the dynamics of the interface at those scales where we observe a well-defined Kolmogorov capacity (Fig. 3) corresponding to a power-law angular frequency (Fig. 5).

Because rolled-up vortex layers are strongly nonhomogeneous we have analyzed the spectral distribution of energy by means of the wavelet transform. This tool enables us to unfold the energy in both the wavelet radius-scale space $(r,l)$ and the wavelet azimuth-scale space $(\phi,l)$. In the $(r,l)$ space the energy $e(r,\phi,l)$ (for a fixed azimuth $\phi$) is organized in blobs located in the vicinity of the curve $l\sim\delta r$, where $\delta r$ denotes the distance between the two adjacent coils closest to the radius $r$ [Eq. (24)]. As time advances, this curve moves towards the small scale region of the wavelet radius-scale space, in a way determined by the Kolmogorov capacity of the spiral. This process is broken when the intercoil distance $\delta r$ reaches the diffusive length scale $\sqrt{\nu t}$, that is, when the viscous core of the spiral reaches the coil of radius $r$. In the physical space the diameter $\rho(t)$ of the inviscid core is given by Eq. (26). In the wavelet radius-scale space the inviscid core of the spiral corresponds to the rectangle domain $\{r<\rho(t)$ and $l<\sqrt{\nu t}\}$ (see Fig. 9). The right top corner of this rectangle (point $A$ in Fig. 9) is the only point of the wavelet radius-scale space where dissipation takes place. The displacement of the curve $l\sim\delta r$ can be investigated in terms of the displacement of the scale $l$ in the wavelet radius-scale space. Indeed, a given scale $l\gg\sqrt{\nu t}$ moves vertically in this space, and the typical duration of this movement is the turnover time $\Omega(\overline{r_l})^{-1}$, where $\overline{r_l}$ is the radius such that $l=\delta r$. By investigating the rate of energy variation $\partial e/\partial t$ we observed that the characteristic time of energy variation at scale $l$ is either $\Omega(\overline{r_l})^{-1}$ or $l^2/\nu$ according to whether viscous effects dominate or not.

In the wavelet azimuth-scale space $(\phi,l)$ the energy $e(r,\phi,l)$ (for a fixed radius $r$) is not localized, as it displays activity everywhere, in contrast with the wavelet radius-scale analysis. Moreover, in the wavelet azimuth-scale space the cutoff induced by viscosity is the shear-augmented diffusive length scale $\Omega(r)\sqrt{\nu t^3}$, and is much larger than $\sqrt{\nu t}$.

The decay of enstrophy and energy of Lundgren's vortex is sensitive to its spiral geometry. In particular, an anomalous decay is observed when the Kolmogorov capacity $D_K$ is large enough. For $D_K>1.75$, the larger the $D_K$ the faster the decay of energy and enstrophy. These properties are in agreement with the fact that the energy spectrum of Lundgren's vortex sheet differs from that of an isolated vortex sheet only for $D_K>1.75$. Indeed, for $D_K\in]1.75,2[$ and large wave numbers $k$, the energy spectrum of Lundgren's vortex scales as $k^{-p}$ with $p=9-4D_K\in]1,2[$, so that the structure is more singular than an isolated vortex sheet in this case, and therefore more sensitive to viscous dissipation.

As in the analysis of rolled-up passive scalar patches (Flohr and Vassilicos [15]), the time range of this anomalous decay (''spiral time range'') is $1\ll\Omega_0 t\ll\mathrm{Re}^{1/3}$, where Re is the Reynolds number defined in Eq. (46), and is therefore rather short in practice, unless $\mathrm{Re}\gg 10^3$.

The spiral investigated in this paper is not strained. We believe that an axisymmetric strain field should modify the distribution and the evolution of the energy in the wavelet position-scale space, and introduce new characteristic time scales due to the radial differential movement. In particular, the movement of the scales in the wavelet radius-scale space might be significantly modified by the strain field. These remarks suggest that the geometry of the spiral in the strained case plays an important role, and that it will be

interesting to extend the analysis presented in this paper to the strained case.


## ACKNOWLEDGMENTS

We wish to thank Dr. F. Nicolleau for interesting discussions and for providing us with a box-counting code. We are grateful for financial support from the Royal Society, the EPSRC, and European Commision's TMR programme.


## APPENDIX A: WAVELET TRANSFORM OF $r\Omega(r)$

In this appendix we calculate the wavelet transform of $r\Omega(r)$ for a wavelet selective in the radial direction. We have

$$\tilde{u}_0(r,\phi,l)=\frac{1}{R}\int_0^R r'\Omega(r')\,\theta\left(\frac{r'-r}{l}\right)dr',$$

that is,

$$\tilde{u}_0(r,\phi,l)=\Omega_0 R^{1/\alpha-1}I_0,$$

where

$$I_0=\int_0^R r'^{\,1-1/\alpha}\theta\left(\frac{r'-r}{l}\right)dr'.$$

By operating the change of variable $y=(r'-r)/l$ we are led to

$$I_0=lr^{1-1/\alpha}\int_{-r/l}^{(R-r)/l}(1+ly/r)^{1-1/\alpha}\theta(y)dy.$$

If the scale is such that

$$\frac{r}{l}\gg 1,$$

and

$$\frac{R-r}{l}\gg 1,$$

then the above integral can be integrated only on the support of the wavelet, say $[-a,+a]$, where $a\sim 1$. In particular, we have $|ly/r|\ll 1$ for all $y\in[-a,+a]$, so that we can expand the integral as

$$I_0\simeq lr^{1-1/\alpha}\left[\int\theta(y)dy+\left(1-\frac{1}{\alpha}\right)\frac{l}{r}\int y\,\theta(y)dy+\frac{1}{2!}\left(1-\frac{1}{\alpha}\right)\left(-\frac{1}{\alpha}\right)\left(\frac{l}{r}\right)^2\int y^2\theta(y)dy+\cdots\right],$$

where all the integrals are taken on the support of the wavelet. The above integrals approximate the moments of the wavelet. If the wavelet is of order $p$ [i.e., $\int y^i\theta(y)dy=0$ for $i=0,1,\ldots,p$ and $\int y^{p+1}\theta(y)dy\neq 0$] the expansion is at leading order

$$I_0\sim lr^{1-1/\alpha}\left(\frac{l}{r}\right)^{p+1},\quad l\ll r.$$

Hence, $\tilde{u}_0$ can be made as small as we want by choosing a large-order wavelet (e.g., a high-order derivative of the Gaussian). In the case of the Morlet wavelet the moments are nonzero, but they are all proportional to $\exp(-m^2/2)$, so that by choosing $m$ large enough we can get rid of the term $\tilde{u}_0$.

## APPENDIX B: CALCULATION OF $\tilde{u}_n$

In this appendix we calculate the wavelet transform of $u_n$ for a wavelet selective in the radial direction, in the case $n\neq 0$. We start from Eq. (18). Let

$$I_n=\int_0^R r'e^{-2in\Omega(r')t}\theta\left(\frac{r'-r}{l}\right)dr'.$$

The integral $I_n$ can be approximated in the limit $l\to 0$ by the method of stationary phases [33] as follows. By inserting expression (16) we are led to

$$I_n=\frac{1}{2i}\int_0^R r'e^{i\psi_1(r')}e^{-(1/2)[(r'-r)/l]^2}dr'+\frac{1}{2i}\int_0^R r'e^{-i\psi_2(r')}e^{-(1/2)[(r'-r)/l]^2}dr',$$

where the phases $\psi_1(r')$ and $\psi_2(r')$ read

$$\psi_1(r')=-2n\Omega(r')t+m\frac{r'-r}{l},\tag{B1}$$

$$\psi_2(r')=+2n\Omega(r')t+m\frac{r'-r}{l}.\tag{B2}$$

When $n<0$, $\psi_1(r')$ has a minimum on $[0,+\infty)$ and $\psi_2(r')$ is monotone. When $n>0$, $\psi_2(r')$ has a minimum on $[0,+\infty)$ and $\psi_1(r')$ is monotone. In both cases the position of the minimum is

$$\overline{r}_{ltn}=R\left(\frac{2|n|\Omega_0 tl}{\alpha mR}\right)^{\alpha/(\alpha+1)}.\tag{B3}$$

The integral in $I_n$ for which the phase is monotone is negligible in comparison to the other integral. In the following we note by $\psi(r')$ the phases $\psi_1(r')$ or $\psi_2(r')$ that has a minimum, that is,

$$\psi(r')=2|n|\Omega(r')t+m\frac{r'-r}{l}.\tag{B4}$$

We approximate $I_n$ by expanding $\psi(r')$ in the vicinity of $\overline{r}_{ltn}$, and by integrating only over an interval centered at $\overline{r}_{ltn}$:

$$I_n\simeq\frac{\pm 1}{2i}\overline{r}_{ltn}e^{-(1/2)[(\overline{r}_{ltn}-r)/l]^2}\times\int_{\overline{r}_{ltn}-\epsilon}^{\overline{r}_{ltn}+\epsilon}e^{\pm i[\psi(\overline{r}_{ltn})+1/2(r'-\overline{r}_{ltn})^2\psi''(\overline{r}_{ltn})]}dr',$$

where $2\epsilon$ is the width of the interval, and the symbol $\pm$ denotes the opposite of the sign of $n$. Because $\psi(\overline{r}_{ltn})$ is a

minimum we have $\psi''(\bar{r}_{ltn})>0$, and by operating the change of variable $y=(r-\bar{r}_{ltn})[\psi''(\bar{r}_{ltn})]^{1/2}$ we get

$$I_n \simeq \frac{\pm 1}{2i}\bar{r}_{ltn} e^{-(1/2)[(\bar{r}_{ltn}-r)/l]^2} e^{\pm i\psi(\bar{r}_{ltn})} \times [\psi''(\bar{r}_{ltn})]^{-1/2} \int_{-\epsilon[\psi''(\bar{r}_{ltn})]^{1/2}}^{+\epsilon[\psi''(\bar{r}_{ltn})]^{1/2}} e^{\pm iy^2/2} dy.$$

In the limit $l\to 0$ we have $\psi''(\bar{r}_{ltn})\to+\infty$, so that the integral in the above equation can be approximated by $\int_{-\infty}^{+\infty}\exp(\pm iy^2/2)=\int_0^{+\infty}\exp(\pm iy/2)y^{-1/2}dy=\sqrt{\pi}(1\pm i)$. Finally,

$$I_n \simeq \frac{\pm 1}{2i}\sqrt{\pi}(1\pm i)\bar{r}_{ltn} e^{-(1/2)[(\bar{r}_{ltn}-r)/l]^2} e^{\pm i\psi(\bar{r}_{ltn})} \times [\psi''(\bar{r}_{ltn})]^{-1/2}.$$

We insert this expression into Eq. (18) to get

$$\tilde{u}_n(r,\phi,l) \simeq \frac{1}{R}e^{2in\phi}\frac{2\alpha-1}{2int}\frac{\pm 1}{2i}\sqrt{\pi}(1\pm i)\bar{r}_{ltn} \times e^{-(1/2)[(\bar{r}_{ltn}-r)/l]^2} e^{\pm i\psi(\bar{r}_{ltn})}[\psi''(\bar{r}_{ltn})]^{-1/2}. \tag{B5}$$

By making use of Eqs. (B4) and (B3) to calculate $\psi''(\bar{r}_{ltn})$ we are led to Eq. (19).

## APPENDIX C: ENERGY SPECTRUM OF LUNDGREN'S VORTEX

The energy spectrum $E(k,t)$ of Lundgren's vortex for $D_K<1.75$ has been calculated by Malik and Vassilicos [37]. These authors use the method of Gilbert [18]. Equation (A5) in [37] reads

$$E(k,t)\sim k^{-3+2(1-\alpha)/(1+\alpha)}\int_1^{n_u} n^{-2(1-\alpha)/(1+\alpha)} = \frac{\alpha+1}{3\alpha-1}k^{-3+2(1-\alpha)/(1+\alpha)}(n_u^{(3\alpha-1)/(\alpha+1)}-1),$$

where $n_u\sim k$ and $n_u\gg 1$ (see Gilbert [18]). For $D_K<1.75$ ($\alpha>1/3$) we get $E(k,t)\sim k^{-2}$, and for $D_K>1.75$ ($\alpha<1/3$) we get $E(k,t)\sim k^{-(1+5\alpha)/(1+\alpha)}$, that is, $E(k,t)\sim k^{4D_K^{-9}}$. The energy spectrum therefore scales as $k^{-p}$ with $1<p<2$ for $D_K>1.75$ and large wave numbers $k$, so that the structure is more singular than an isolated vortex layer.


[1] O. Cadot, S. Douady, and Y. Couder, Phys. Fluids **7**, 630 (1995).
[2] Z. S. She, E. Jackson, and S. A. Orszag, Nature (London) **344**, 226 (1990).
[3] G. R. Ruetsch and M. R. Maxey, Phys. Fluids A **3**, 1587 (1991).
[4] A. P. Vincent and M. Meneguzzi, J. Fluid Mech. **225**, 1 (1991).
[5] J. Jiménez, A. A. Wray, P. G. Saffman, and R. S. Rogallo, J. Fluid Mech. **255**, 65 (1993).
[6] P. G. Saffman, *Vortex Dynamics* (Cambridge University Press, Cambridge, England, 1992).
[7] M. Meneguzzi and A. Vincent, J. Fluid Mech. **258**, 245 (1994).
[8] T. S. Lundgren, Phys. Fluids A **5**, 1472 (1993).
[9] T. S. Lundgren, Phys. Fluids **25**, 2193 (1982).
[10] S. J. Lin and G. M. Corcos, J. Fluid Mech. **153**, 31 (1984).
[11] J. C. Neu, J. Fluid Mech. **143**, 253 (1984).
[12] T. Passot, H. Politano, P. L. Sulem, J. R. Angilella, and M. Meneguzzi, J. Fluid Mech. **282**, 313 (1995).
[13] F. Nicolleau and J. C. Vassilicos, Philos. Trans. R. Soc. (to be published).
[14] J. C. Vassilicos, Phys. Rev. E **52**, 5753 (1995).
[15] P. Flohr and J. C. Vassilicos, J. Fluid Mech. **348**, 295 (1997).
[16] J. R. Angilella and J. C. Vassilicos, Physica D **124**, 23 (1998).
[17] H. K. Moffatt, in *Turbulence and Chaotic Phenomena in Fluids*, edited by T. Tatsumi (Elsevier, Amsterdam, 1984), p. 223.
[18] A. D. Gilbert, J. Fluid Mech. **193**, 475 (1988).
[19] A. D. Gilbert, Phys. Fluids **5**, 2831 (1993).
[20] J. C. Vassilicos and J. C. R. Hunt, Proc. R. Soc. London, Ser. A **435**, 505 (1991).
[21] M. Farge, Annu. Rev. Fluid Mech. **24**, 395 (1992).
[22] C. Meneveau, J. Fluid Mech. **232**, 469 (1991).
[23] T. Kambe, Physica D **37**, 463 (1989).
[24] K. J. Falconer, *Fractal Geometry—Mathematical Foundations and Applications* (Wiley, New York, 1990).
[25] D. I. Pullin and P. G. Saffman, Phys. Fluids A **5**, 126 (1993).
[26] J. C. Vassilicos and J. G. Brasseur, Phys. Rev. E **54**, 467 (1996).
[27] R. Krasny, J. Comput. Phys. **65**, 292 (1986).
[28] R. Krasny, Fluid Dyn. Res. **3**, 93 (1988).
[29] D. W. Moore, Proc. R. Soc. London, Ser. A **365**, 105 (1979).
[30] H. K. Moffatt, in *Fractals, Wavelets and Fourier Transforms: New Developments and New Applications*, edited by M. Farge, J. C. Hunt and J. C. Vassilicos (Clarendon Press, Oxford, 1993), pp. 317–324.
[31] R. M. Everson and K. R. Sreenivasan, Proc. R. Soc. London, Ser. A **437**, 391 (1992).
[32] C. Gasquet and P. Witomski, *Analyse de Fourier et applications* (Masson, Paris, 1990).
[33] J. C. R. Hunt, N. K. Kevlahan, J. C. Vassilicos, and M. Farge, in *Fractals, Wavelets and Fourier Transforms: New Developments and New Applications* (Ref. [30]), pp. 1–38.
[34] D. W. Moore and P. G. Saffman, Proc. R. Soc. London, Ser. A **333**, 491 (1973).
[35] P. B. Rhines and W. R. Young, J. Fluid Mech. **133**, 133 (1983).
[36] *Handbook of Mathematical Functions*, edited by M. Abramowitz and I. A. Stegun (Dover, New York, 1965).
[37] N. A. Malik and J. C. Vassilicos, J. Fluid Mech. **326**, 417 (1996).